Fracture Mechanics of Concrete and Concrete Structures - Recent Advances in Fracture Mechanics of Concrete - B. H. Oh, et al.(eds)

Anisotropic loading criterion for depicting loading induced anisotropy in concrete

A. Yong-Hak Lee & Yeong-Seong Park
Department of Civil Engineering, Konkuk University, Seoul, Korea

B. Young-Tae Joo
MidasITl Co., Soengnam, Korea

C. Won-Jin Sung
GS E&C, Seoul, Korea

D. Byeong-Su Kang
SK E&C, Seoul, Korea

ABSTRACT : The traditional isotropic failure description of a self-similar loading surface exhibits severe limitations on depicting the loading-induced anisotropy. In this paper, an anisotropic formulation to model triaxial behavior of concrete is presented in the framework of classical theory of plasticity. For this purpose, a triaxial anisotropic loading function that distinguishes Mode I-dominated and Mode II-dominated behaviors is introduced in terms of three invariants. Two internal state variables associated with volumetric and deviatoric control the evolution of loading surface. For this purpose, total plastic strains are decomposed into volumetric and deviatoric components based on normality condition between the two components. As a conclusion, limitations of adopting isotropic formulation are addressed through numerical predictions of two non-proportional loading histories that are in inverse sequence.

1 INTRODUCTION

In case of non-proportional load histories where compressive-dominated load is applied and subsequently unloaded, and tensile-dominated load is reloaded, mechanical behavior under the latter loading is pretty much influenced by the former loading history due to the mixed type of internal damage formed during the former loading. Behavior of concrete under this type of non-proportional loading may be well predicted by isotropic description of constitutive model due to isotropically induced internal damage (Pramono & Willam (1989), Yazdani & Schreyer (1990), Bazant (2000), Imran & Pantazoupoulou (2001), Sfer et al. (2002), Grassl et al. (2002), Papanikolaou & Kappos (2007), Cervenka & Papanikolaou (2008)). However, this is not a case if the loading sequence is reversed where tensile-dominated load is applied prior to compressive-dominated load. In this loading sequence, the inelastic damage developed under crack-opening circumstance of tensile-dominated load hardly affects the inelastic behavior under crack-closing circumstance of compressive-dominated load. Loading-induced anisotropy is modeled in the framework of classical theory of plasticity to remedy limitations encountered when isotropic evolution law of self-similar loading surface applies to concrete structures subjected to non-proportional and non-monotonic load histories along load paths.

Adopting a conventional flow theory of plasticity, the entire inelastic response is monitored by single hardening (or softening) parameter defined as a function of effective plastic strain that has a mathematical meaning of magnitude of plastic strain vector. Energy dissipative mechanism along this conventional concept does not distinguish the difference between Mode I type of decohesion and Mode II type of friction and thereby, leads to a self-similar evolution of loading surface. In the current formulation, the progressive failure of concrete is prescribed by two independent failure mechanisms of cohesion and friction that represent energy dissipations due to mode I type of tesile splitting and mode II type of shear faulting. The two failure mechanisms are incorporated in a failure criterion by introducing two control parameters of cohesion-related and friction-related internal state variables. The main difficulty of adopting two plastic internal state variables arises when the amount of energy dissipated during inelastic process is decomposed of cohesion and friction components. For that reason, total plastic flow vec-

tor is decomposed into volumetric and deviatoric components based on normality condition between the two components. Upon calculating effective plastic strains for the two flow components, two control parameters with regards to cohesion and friction are expressed in term of corresponding effective plastic strains. In this conjnction, the lading function differentiates the evolution law due to hydrostatic behavior from that due to deviatoric behavior by the two control parameters.

This type of plasticity modeling requires an invariant formulation of triaxial loading function where the first and second invariants are decoupled. For this purpose, a triaxial anisotropic loading function is introduced in terms of three invariants. The fundamental difference between isotropic and anisotropic loading descriptions are addressed by comparing the model performances predicted for two non-proportional load histories in which tension is applied in one direction and unloaded and compression is reloaded into the opposite direction, and the other loading sequence is in inverse way to the loading history.

2 FLOW RULES

2.1 *Decomposition of plastic strains*

The two energy dissipative mechanisms of cohesion and friction are independently incorporated in the current formulation framework to allow the evolution of loading surface in an anisotropic way. The main difficulty encountered in accepting the two-control parameter concept arises when total amount of dissipated energy is decomposed into the counterparts of cohesion and friction. To resolve the problem, normal vector $\mathbf{m}$ of plastic potential Q is decomposed into the gradients of $\mathbf{m}_{\mathrm{h}}$ and $\mathbf{m}_{\mathrm{f}}$ along hydrostatic and deviatoric stress axes defined in meridian plane, respectively. (Fig. 1)

$$\mathbf{m} = \mathbf{m}_{\mathrm{h}} + \mathbf{m}_{\mathrm{f}} \tag{1}$$

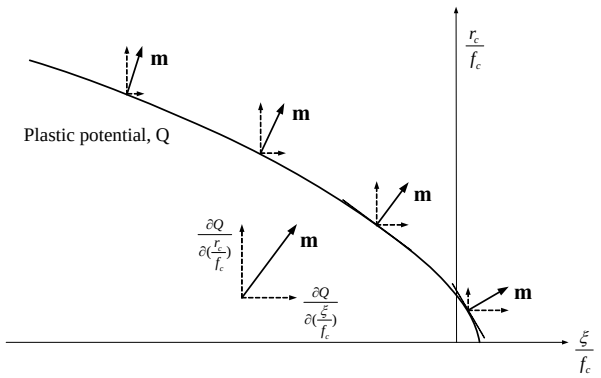

Figure 1. Components of normal vector to plastic potential Q.

Based on the direction vector of plastic flow in Equation (1), total plastic strain $\dot{\boldsymbol{\varepsilon}}_{\mathrm{p}}$ can be decomposed into the corresponding hydrostatic and deviatoric components of $\dot{\boldsymbol{\varepsilon}}_{\mathrm{ph}}$ and $\dot{\boldsymbol{\varepsilon}}_{\mathrm{pf}}$ as

$$\dot{\boldsymbol{\varepsilon}}_{\mathrm{p}} = \dot{\lambda}\mathbf{m} = \dot{\boldsymbol{\varepsilon}}_{\mathrm{ph}} + \dot{\boldsymbol{\varepsilon}}_{\mathrm{pf}} \tag{2}$$

where the plastic multiplier $\dot{\lambda}$ controls the magnitude of the plastic flow.

Two independent scalar-valued effective plastic strains of $\dot{\varepsilon}_{ph}$ and $\dot{\varepsilon}_{pf}$ memorize inelastic deformation histories. Taking inner product in Equation (2) and applying normality condition between the two gradients of $\mathbf{m}_{\mathrm{h}}$ and $\mathbf{m}_{\mathrm{f}}$ lead to an algebraic Equation to determine the relationship among the three equivalent plastic strain values of $\dot{\varepsilon}_p$, $\dot{\varepsilon}_{ph}$ and $\dot{\varepsilon}_{pf}$ as

$$(\dot{\varepsilon}_p)^2 = (\dot{\varepsilon}_{ph})^2 + (\dot{\varepsilon}_{pf})^2 \tag{3}$$

The equivalent plastic strains of $\dot{\varepsilon}_p$, $\dot{\varepsilon}_{ph}$ and $\dot{\varepsilon}_{pf}$ in Equation (3) are readily defined in terms of vector norms as

$$\dot{\varepsilon}_p = \dot{\lambda}\|\mathbf{m}\|,\ \dot{\varepsilon}_{ph} = \dot{\lambda}\|\mathbf{m}_{\mathrm{h}}\|,\ \dot{\varepsilon}_{pf} = \dot{\lambda}\|\mathbf{m}_{\mathrm{f}}\| \tag{4}$$

where vector norm $\|\mathbf{m}\| = \sqrt{\mathbf{m}:\mathbf{m}}$. Furthermore, ratios among the three effective plastic strains are obtained from Equation (4) as

$$\dot{\varepsilon}_{ph} = \frac{\|\mathbf{m}_{\mathrm{h}}\|}{\|\mathbf{m}\|}\dot{\varepsilon}_p,\quad \dot{\varepsilon}_{pf} = \frac{\|\mathbf{m}_{\mathrm{f}}\|}{\|\mathbf{m}\|}\dot{\varepsilon}_p \tag{5}$$

The internal state variables of $\dot{\varepsilon}_{ph}$ and $\dot{\varepsilon}_{pf}$ in Equation (5) are linked with hardening parameters to control the evolution of loading surface depending on the amounts of energies dissipated during decohesive and friactional fracture processes.

2.2 *Plastic flow direction*

Dilatant problem in an associated flow rule is primarily due to the gradient along hydrostatic stress axis of loading surface defined as $\partial F/(\partial\xi/f_c)$ in Figure 2. In this paper, the plastic flow vector $\mathbf{m}$ is approximated by adjusting the hydrostatic component of gradient $\mathbf{n}$. Figure 2 illustrates the variation of plastic flow direction $\mathbf{m}$ in which the gradient component of loading surface along hydrostatic stress axis decreases when confining pressure increases.

Denoting direction angle of normal vector $\mathbf{n}$ as θ_n, direction angle of platic flow vector θ_m in Figure 2 is expressed as

$$\theta_m = \theta_n(1+\alpha_n) \tag{6}$$

where α_n depicts the intensity of non-associated flow and is defined in terms of hardening and softening strength parameters, and hydrostatic pressure to prescribe non-associativity depending on level of inelastic deformation and volumetric confinement

$$\alpha_c = \left(k_h + 1 - c_h\right)\frac{\left|\xi / f_c\right|}{\left|\left(\xi / f_c\right)_{non}\right|}, \quad \frac{\left|\xi / f_c\right|}{\left|\left(\xi / f_c\right)_{non}\right|} \le 1 \tag{7}$$

where k_h and c_h are hardening and softening strength parameters related to volumetric part, respectively, ξ is the first invariant, and $(\xi / f_c)_{non}$ is a reference value to define the transition region from associated to strong non-associated.

Upon determining the direction angle of plastic flow θ_m, the components of plastic flow vector $\mathbf{m}$ along hydrostatic and deviatoric stress axes, $\mathbf{m_h}$ and $\mathbf{m_f}$, are calculated as

$$\mathbf{m_f} = \mathbf{n_f}; \quad \mathbf{m_h} = (\tan^{-1}\theta_m)\mathbf{n_h} \tag{8}$$

where normal vector components of $\mathbf{n_h}$ and $\mathbf{n_f}$ are calculated by applying the chain rule of differentiation to loading function F that are expressed in terms of the hydrostatic length ξ, the deviatoric length r and the angle of similarity θ in deviatoric plane and thereby, expressed in form of $F = F(\xi, r, \theta)$:

$$\mathbf{n_h} = \frac{\partial F}{\partial\left(\xi / f_c\right)}\frac{\partial\left(\xi / f_c\right)}{\partial \boldsymbol{\sigma}}; \quad \mathbf{n_f} = \frac{\partial F}{\partial\left(r / f_c\right)}\frac{\partial\left(r / f_c\right)}{\partial \boldsymbol{\sigma}} \tag{9}$$

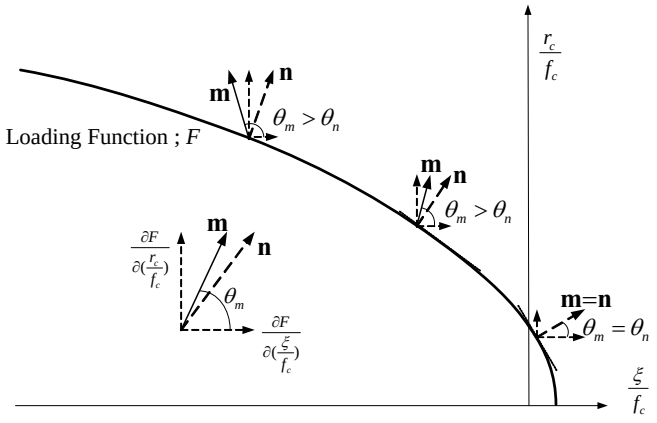

Figure 2. Direction of plastic flows on loading surface.

3 ELASTO-PLASTIC CONTINUUM TANGENT OPERATOR

Assuming a three invariants-based loading function with two control parameters, the implicit form of loading function is expressed as

$$F = F\{\xi, r, \theta, K_h(k_h, c_h), K_f(k_f, c_f)\} \tag{10}$$

ξ, r and θ in Equation (10) are hydrostatic length, deviatoric length and Lode angle, respectively, define Haigh-Westergaard stress space.

Two control parameters of k_h and k_f (or c_h and c_f in case of softening) in Equation (10) scale the amounts of inelastic actions activated on volumetric and deviatoric parts, respectively, and control the evolution of loading surface. Thereby, those parameters are expressed as functions of equivalent plastic strains of $\dot{\varepsilon}_{ph}$ and $\dot{\varepsilon}_{pf}$ in Equation (5)

$$k_h = k_h(\varepsilon_{ph}),\ c_h = c_h(\varepsilon_{ph}),\ k_f = k_f(\varepsilon_{pf}),\ c_f = c_f(\varepsilon_{pf}) \tag{11}$$

In case of softening, the two softening parameters of c_h and c_f may be formulated according to the regularization methods for localized deformations (Pramono & Willam (1989), Lee & Willam (1997), Imran & Pantazopoulou (2001) among others). K_h and K_f in Equation (10) prescribe the general implicit expression for the control parameters.

Truncated Taylor series expansion of Equation (10) leads to the linearized format of consistency

$$\dot{F} = \frac{\partial F}{\partial \boldsymbol{\sigma}} : \dot{\boldsymbol{\sigma}} + \frac{\partial F}{\partial K_h}\frac{\partial K_h}{\partial k_h}\frac{\partial k_h}{\partial \varepsilon_{ph}}\frac{\partial \varepsilon_{ph}}{\partial \varepsilon_p}\dot{\varepsilon}_p + \frac{\partial F}{\partial K_f}\frac{\partial K_f}{\partial k_f}\frac{\partial k_f}{\partial \varepsilon_{pf}}\frac{\partial \varepsilon_{pf}}{\partial \varepsilon_p}\dot{\varepsilon}_p = 0 \tag{12}$$

The total strain rate may be decomposed into independent elastic and plastic components in the case of infinitesimal deformation

$$\dot{\boldsymbol{\varepsilon}} = \dot{\boldsymbol{\varepsilon}}_{\mathrm{e}} + \dot{\boldsymbol{\varepsilon}}_{\mathrm{p}} \tag{13}$$

Assuming that the elastic response may be described by the linear isotropic operator $\mathbf{E}$, the final stress rate $\dot{\boldsymbol{\sigma}}$ returned from the stress state elastically predicted is

$$\dot{\boldsymbol{\sigma}} = \mathbf{E} : \dot{\boldsymbol{\varepsilon}} - \dot{\lambda}\,\mathbf{E} : \mathbf{m} \tag{14}$$

Substituting Equations (1), (5) & (14) into (12) and solving with respect to plastic multiplier $\dot{\lambda}$, the plastic multipler $\dot{\lambda}$ is calculated as

$$\dot{\lambda} = \frac{\mathbf{n} : \mathbf{E} : \dot{\boldsymbol{\varepsilon}}}{-\left\{H_h \left\|\mathbf{m}_{\mathrm{h}}\right\| + H_f \left\|\mathbf{m}_{\mathrm{f}}\right\|\right\} + \mathbf{n} : \mathbf{E} : \mathbf{m}} \tag{15}$$

where H_h and H_f are the hardening moduli defined from Equation (12). The elasto-pastic tangent operator $\mathbf{E}_{\mathrm{ep}}$ is readily developed when the plastic multipler $\dot{\lambda}$ Equation (15) is substituted into Equation (14)

$$\mathbf{E}_{\mathrm{ep}} = \mathbf{E} - \frac{\mathbf{E} : \mathbf{m} \otimes \mathbf{n} : \mathbf{E}}{-\left\{H_h \left\|\mathbf{m}_{\mathrm{h}}\right\| + H_f \left\|\mathbf{m}_{\mathrm{f}}\right\|\right\} + \mathbf{n} : \mathbf{E} : \mathbf{m}} \tag{16}$$

4 LOADING FUNCTION WITH TWO CONTROL PARAMETERS

4.1 *Triaxial loading function*

The triaxial loading function presented here is based on the elliptic approximation of deviatoric plane of Willam & Warnke (1975). Based on the work, the deviatoric length $r(\theta)$ at the position with θ of Lode angle in a deviatoric plane is expressed in terms of tensile meridian $r_t(=r(\theta=0))$ and compressive meridian $r_c(=r(\theta=\pi/3))$, Lode angle θ

$$r(\theta)=\frac{2r_c(r_c^2-r_t^2)\cos\theta+r_c(2r_t-r_c)[4(r_c^2-r_t^2)\cos^2\theta+5r_t^2-4r_tr_c]^{\frac{1}{2}}}{4(r_c^2-r_t^2)\cos^2\theta+(r_c-2r_t)} \quad (17)$$

Introducing eccentricity $e_c\ (=r_t/r_c)$ and deviatoric shape function $g_c(\theta)$ into Equation (17), and normalizing with respect to uniaxial compressive strength f_c, a general form of loading function F is obtained

$$F=\frac{r(\theta)}{f_c g_c(\theta)}-\frac{r_c}{f_c} \quad (18)$$

where e_c ranges between 0.5 for tensile or low confining pressure to 1 for high confining pressure. To approximate the compressive meridian in Equation (18), three data points of A, B and C are selected in meridian plane of Figure 3 in which point A defines the triaxial tensile strength, B the low confining pressure, C the high confining pressure, and n the cap point to close loading surface.

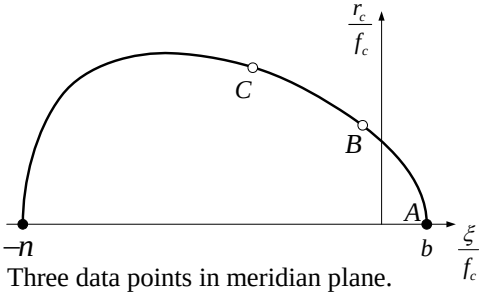

Figure 3. Three data points in meridian plane.

Loading function that maintains C^1 continuity and convexity condition throughout the entire response regime was obtained by combining two independent functions that describe the conical bulge along deviatoric axis and the closing cap along compressive hydrostatic axis as shown in Figure 3.

$$F(\xi,r,\theta)=\left[\left\{\frac{r(\theta)}{f_c g_c(\theta)}-A_1\right\}^2+a\left(b-\frac{\xi}{f_c}\right)-(A_2)^2\left(\frac{\xi}{f_c}+n\right)\right]^2+$$
$$4(A_2)^2 a\left(b-\frac{\xi}{f_c}\right)\left(\frac{\xi}{f_c}+n\right)=0 \quad (19)$$

where $A_1=c\{(\xi/f_c)+n\}-\{-a(b+n)\}^{1/2}$ and $A_2=a^{1/2}-c(b+n)^{1/2}$. Initial elastic and maximum states of loading envelope of Equation (19) are defined by determining the initial and maximum values of the four parameters of a, c, n, and b in Equation (19) from the three types of experiments related to the three points of A, B and C that correspond to equi-triaxial tension, uniaxial compression and high confininging pressure, respectively. The maximum value of cap parameter n may be chosen to be an enough large value to take account of concrete character that concrete does not fail under hydrostatic pressure. $a_{\max}$, $c_{\max}$, $n_{\max}$, and $b_{\max}$, and $a_{\min}$, $c_{\min}$, $n_{\min}$, and $b_{\min}$ are the maximum and minimum values of the four parameters a, c, n, respectively.

4.2 *Hardening and softening rules*

A non-dimensionalized hardening parameter monitors the inelastic deformation process in hardening regime in term of the scalar-valued kinematic variable ε_p as

$$k=\frac{2}{\varepsilon_0}\left[\sqrt{2\varepsilon_0\varepsilon_p}-\varepsilon_p\right] \quad (20)$$

where ε_o is a ductility measure to incorporate the effect of confining pressure.

To align with the two control parameter concept of Equation (5), two hardening parameters of volumetric-related and deviatoric-related are introduced in a similar fashion of Equation (20)

$$k_h=\frac{2}{\varepsilon_0}\left[\sqrt{2\varepsilon_0\varepsilon_{ph}}-\varepsilon_{ph}\right],\quad k_f=\frac{2}{\varepsilon_0}\left[\sqrt{2\varepsilon_0\varepsilon_{pf}}-\varepsilon_{pf}\right] \quad (21)$$

Combining two hardening parameters k_h and k_f with the minima and maxima of the four parameters leads to anisotropic evolution law of loading function where the inelastic deforming process is decomposed into volumetric and deviatoric parts

$$k_a=a_{\min}+k_f(a_{\max}-a_{\min}),\quad k_c=c_{\min}+k_f(c_{\max}-c_{\min})$$
$$k_n=n_{\min}+k_f^2(n_{\max}-n_{\min}),\quad k_b=b_{\min}+k_h(b_{\max}-b_{\min}) \quad (22)$$

It is noted in Equation (22) that a, c and n parameters are linked with friction-related hardening parameter k_h and b is linked with cohesion-related hardening parameter k_f.

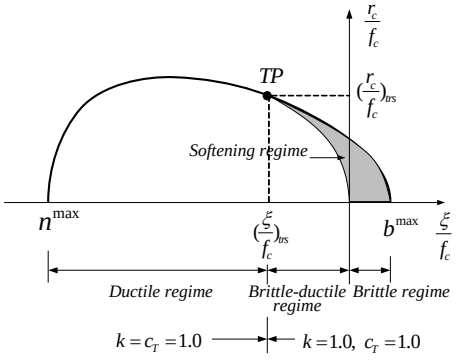

Figure 4. Ductile and brittle response regimes.

In fracture mechanics, the degradation of tensile strength f_t is invariably related to the crack opening displacement u_p rather than tensile fracture strain ε_p. An exponential function approximates the degradation of tensile strength as

$$c_T = \frac{\sigma_t}{f_t} = e^{-c_o u_p} \tag{16}$$

where c_o is the ductility measure for softening response. The missing link between the crack opening displacement u_p and the tensile fracture strain ε_p follows the fracture energy arguments of Lee and Willam (1997a, b). Similarly to anisotropic evolution law of loading surface in hardening regime of Equation (22), two control parameters of c_h and c_f are introduced to decompose the total inelastic deforming process into volumetric and deviatoric parts

$$c_h = e^{-c_{oh} u_{ph}}, \quad c_f = e^{-c_{of} u_{pf}} \tag{17}$$

Softening effect decreases as loading becomes compressive-dominated and even only the hardening behavior takes place under high confinement. Transition point (TP) in Figure 4 delimits the maximum envelope without softening and the residual envelope with softening.

Relationships among the three parameters of a, c and b, and the two softening parameters c_h and c_f of Equation (24) are linearly approximated to define an anisotropic evolution law of loading surface

$$\begin{aligned} k_b &= b^{\max}\left\{1 - R_{ab}(1-c_h)\right\} \\ k_a &= (a^{\max} - a^{\min})\left\{1 - R_{ab}(1-c_f)\right\} + a^{\min} \\ k_c &= (c^{\max} - c^{\min})\left\{1 - R_{ab}(1-c_f)\right\} + c^{\min} \end{aligned} \tag{18}$$

The strength reduction function of R_{ab} in Equation (25) is defined as a quadratic form in term of hydrostatic stress to maintain smooth transition at transition point and to enforce no softening when $(\xi / f_c) \le (\xi / f_c)_{trs}$ as shown in Figure 5.

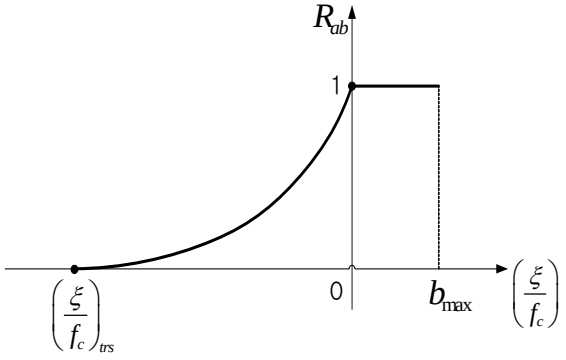

Figure 5. Strength Reduction Function R_{ab}.

The gradual expansion and contraction of loading function of Equation (19) are investigated for the anisotropic case of Equations (22)-(25) as well as the isotropic case which is the single control parameter representation of (21) and (22), and (24) and (25). The required input parameter values were calculated based on the experimental results of Launay & Gachon (1972). Figure 6 shows the isotropic evolution of loading surface where the hardening envelope in Figure 6(a) was obtained by increasing the hardening parameter value k from 0 to 1.0 and the softening envelope in Figure 6(b) was obtained by decreasing the softening parameter value c_T from 1.0 to 0. It is noted that the loading function maintains C^1-continuity through the entire response regime. Choosing $n^{\max} = 50$ is large enough to compensate for the contradiction of which concrete does not fail under hydrostatic pressure. The value of $(\xi / f_c)_{trs} = -1.0$ to define transition point is taken from the experimental result of Smith (1987). It is noteworthy that the strength reduction function R_{ab} plays a role to control no softening in ductile regime, smooth transition through residual region and softening in brittle regime.

Anisotropic evolution of loading surface is shown in Figure 7 in which loading along positive hydrostatic axis takes place prior to that along negative hydrostatic axis with changing the values of two control parameters c_h and k_f from 1.0 and 1.0 to 0 and 1.0, respectively. Then loading takes place along negative hydrostatic axis with changing the values of c_h and k_f from 0 and 0 to 0 and 1, respectively.

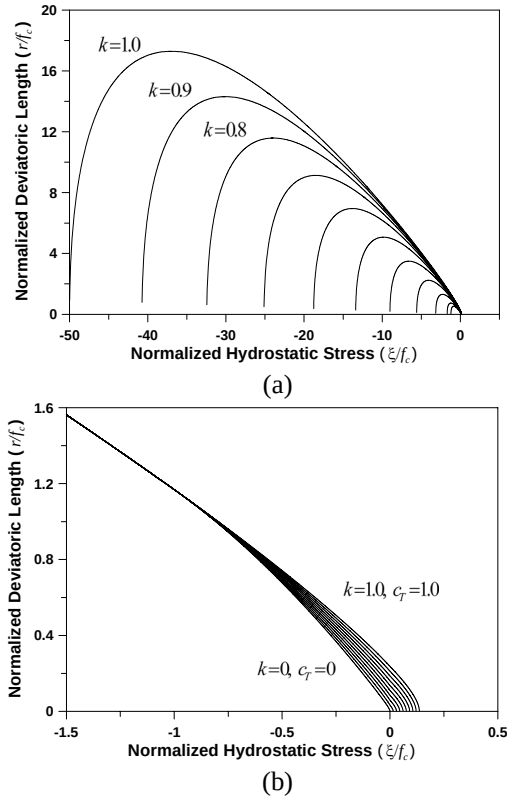

Figure 6. Isotropic Evolution of Four-Parameter Loading Function (a) Hardening, (b) Softening.

It is interesting to observe that loading along positive hydrostatic axis results in only decrease of cohesion parameter k_b due to decrease of c_h value from 1 to 0, while the friction parameters k_a and k_c remain their minimum values. Upon reaching the value of c_h into its minimum 0, change of loading direction into negative hydrostatic axis leads to a similar evolution.

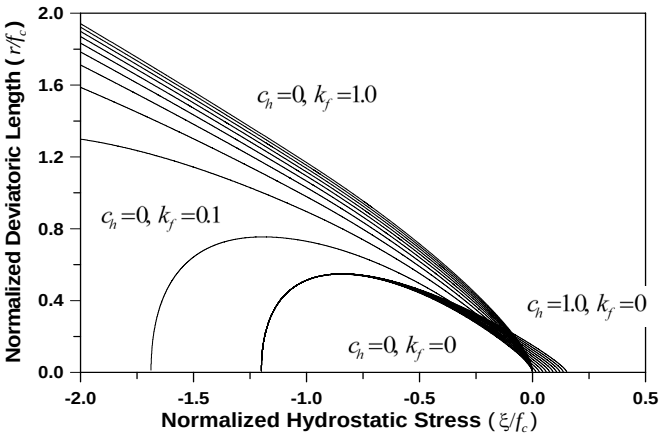

Figure 7. Anisotropic Evolution of Four-Parameter Loading Function.

5 MODEL PREDICTIONS

The present triaxial concrete constitutive model was implemented to investigate the model performance by comparing the experimental results of Smith et al. (1989) that had been performed on a 33.5 MPa uniaxial compressive strength concrete with various levels of lateral confining pressures including 0.7, 3.4, 6.8, 13.7, 20.5, 27.3, and 34.2 MPa. Among all the parameter values required for the constitutive and material descriptions, the constitutive parameter values were obtained from the test results of Launay & Gachon (1972). The parameter values used in the calibration are listed in Table 1.

Table 1. Parameter Values for $f_c = 33.5$ MPa Concrete.

Parameter	Value
Elastic modulus, E	19140 MPa
Poisson's ratio, ν	0.2
Compressive strength, f_c	33.5 MPa
Tensile strength, f_t	3.4 MPa
Transition point, $(\xi / f_c)_{trs}$	-3.0
Max. and min. values of point C in Figure 3	$(\xi / f_c)_{\max} = -5.0$ $(r / f_c)_{\max} = 8.0$ $(\xi / f_c)_{\min} = -1.0$ $(r / f_c)_{\max} = 0.3$
Max. and min. values of closing pont n	$n_{\max} = -200$ $n_{\min} = -1.2$
Ductility measure ε_o in uniaxial compression	0.006
Ductility measure c_o in uniaxial comp. and ten.	c_o *at comp.* $= 17$ c_o *at ten.* $= 500$

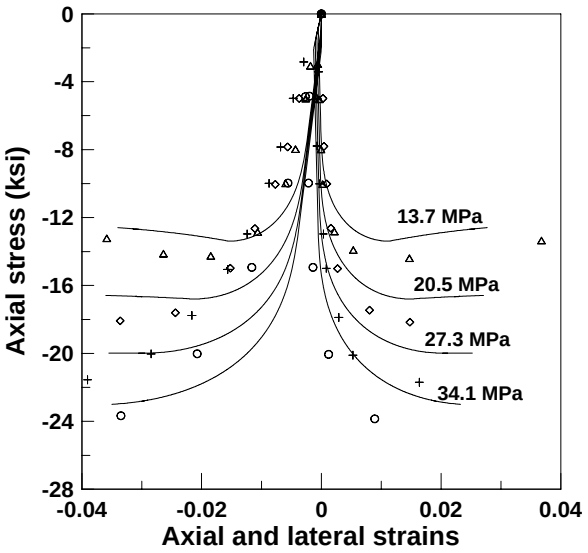

Figure 8. Comparison between numerical and experimental results for low confinement cases (confining pressures = 0, 0.7, 3.4, 6.8 MPa).

Figure 8-9 compare the numerical and experimental results of Smith et al. (1989) for various levels of low and high confinements. The constitutive model well predicts the increases of maximum stress, residual stress level and ductility with the increase of confining pressure. Non-associated plastic flow formulation presented in this paper can be evaluated by investigating the variation of lateral strain according to the increase of lateral pressure. It is observed from Figures 8 and 9 that the lateral strain is well controlled with the increase of confinement level where dilatant behavior is predominant when confinement level is low and it becomes volume compaction with the increase of confinement level. This observation clearly explains the robustness of the present flow formulation.

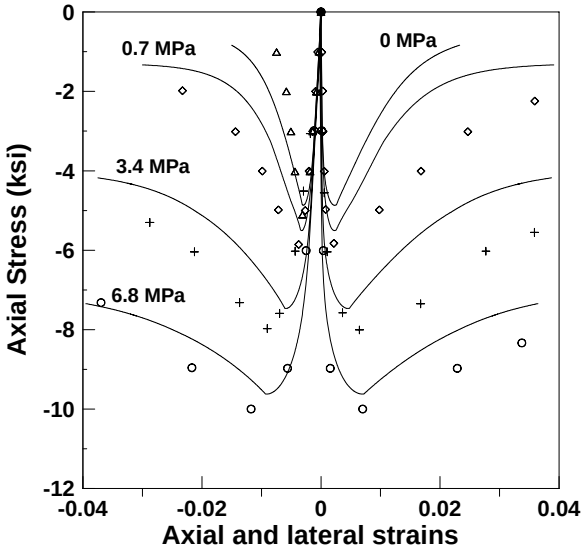

Figure 9. Comparison between numerical and experimental results for high confinement cases (confining pressures = 13.6, 20.5, 27.3, 34.1 MPa).

Two cases of non-proportional loading sequences are analyzed to investigate the model performances

of isotropic and anisotropic evolution laws of loading surface. The isotropic formulation is based on single control parameter using Equations (20) & (23), and the anisotropic formulation is based two control using Equations (21) & (24). In the first loading sequence, uniaxial tension load is applied until tensile cracking is fully developed by letting the stress be in the softening range and subsequently unloaded and reloaded to uniaxial compressive direction to close the tensile crack. In the second loading sequence, uniaxial compressive load is applied until mixed mode type of fracture is developed and subsequently unloaded and reloaded to uniaxial tension direction. Figure 10 compares the prediction results using isotropic and anisotropic formulations for the first loading sequence. Isotropic formulation predicts the compressive behavior in hardening regime as entirely elastic. This is clearly contrary to the internal state of concrete with crack closed and fully recovered from tensile crack-opening during unloading from tensile-loading. However, anisotropic formulation predicts the compressive behavior as inelastic with hardening in hardening regime depending on the degree of tensile crack-opening. Figure 11 compares the prediction results using isotropic and anisotropic formulations for the second loading sequence. In the second loading sequence, uniaxial compressive load is applied until the stress reaches 98% of the compressive strength and unloaded and reloaded to uniaxial tension direction to induce enough opening of tensile crack. In case of isotropic formulation, the tensile strength is still preserved even if concrete experienced almost peak stress and large enough internal damage during the compressive loading. On the other hand, anisotropic formulation reduces the tensile strength to 15% of the original strength.

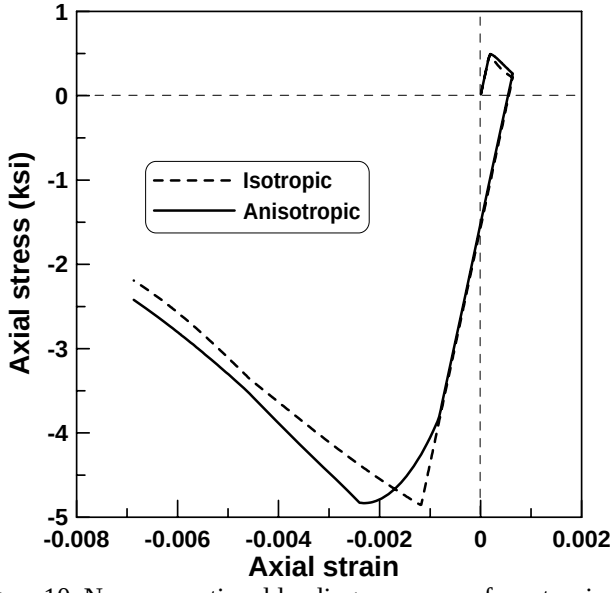

Figure 10. Non-proportional loading sequence : from tension to compression.

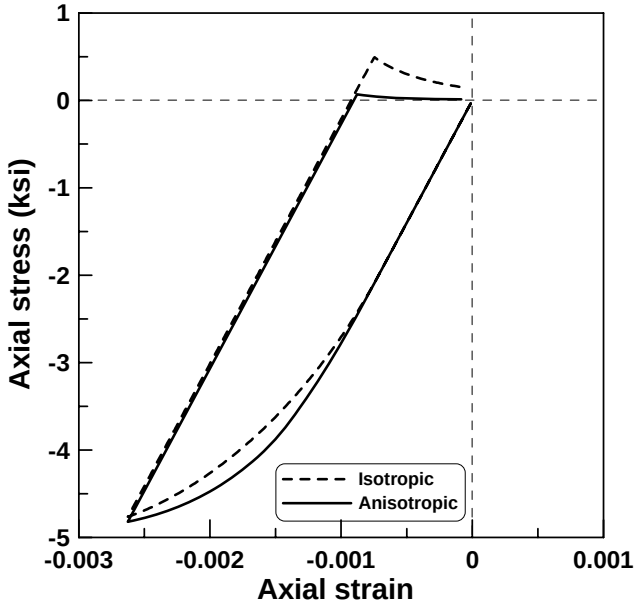

Figure 11. Non-proportional loading sequence : from compression to tension.

6 CONCLUSIONS

Anisotropy due to directional loading in concrete was modeled in the present constitutive formulation by introducing two control parameters. The main objective of two control parameter concept was to depict a progressive failure process of concrete with two independent failure mechanisms of Mode I type of decohesion and Mode II type of friction. Two effective plastic strains to define two control parameters were obtained by decomposing the total plastic strain tensor into volumetric and deviatoric components based on normality condition between the two flow components. Direction of plastic flow vector was obtained from non-associated formulation without resorting to plastic potential function where the flow vector component along hydrostatic axis was modified to control dilatancy effect observed under congining pressure. This type of non-associated formulation was successfully completed owing to the decomposition concept of plastic flow vector with normality condition. The present formulation predicted the triaxial concrete experiments that had been performed for various levels of confining pressure. The main difference between isotropic and anisotropic formulations was highlighted for non-proportional loading history analyses.

ACKNOWLEDGEMENT

This research was supported by a grant (code-Technology Innovation-A01) from Construction Technology Innovation Program funded by Ministry of Construction & Transportation of Korean government.

REFERENCES

Bazant, Z. P., Caner, F. C., Carol, I., Adley, M. D., Akers, S. A., 2000, "Microplane model M4 for concrete. I : Formulation with work-conjugate deviatoric stress," *J. of Engrg. Mech.*, ASCE, V.126, No.9, pp.944-953.

Cervenka, J., & Papanikolaou, V. K., 2008 "Three dimensional combined fracture–plastic material model for concrete," *Int. J. of Plasticity*, V. 24, pp.2192-2220.

Cicekli, U., Voyiadjis, G. Z., Abu Al-Rub, R. K., 2007 "A plasticity and anisotropic damage model for plain concrete," *Int. J. Plasticity*, V.23, pp.1874–1900.

Grassl, P., Lundgren, K., & Gylltoft, K., 2002 "Concrete in compression: a plasticity theory with a novel hardening law," *Int. J. of Solids and Str.*, V.39, pp.5202-5223.

Imran, I, & Pantazopoulou, S. J., 2001 "Plasticity Model for Concrete unider Triaxial Compression," *J. of Engrg. Mech.*, ASCE, V.127, No.4, pp.281-290.

Imran, I. & Pantazopoulou, S. J., 1996 ''Experimental study of plain concrete under triaxial stresses.'' *ACI Mater. J.*, V.93, pp.589–601.

Launay, P., & Gachon, H., 1972. "Strain and ultimate strength of concrete under triaxial stress." *ACI Special Publ.* SP-34.,

Lee, Y.-H & Willam, K. J., 1997 "Mechanical Properties of Concrete in Uniaxial Compression," *ACI Materials J.*, V.94, No.6, (a), pp.457-471.

Lee, Y.-H., & Willam, K. J., 1997 "Anisotropic vertex plasticity formulation for concrete in-plane stress," *J. of Engrg. Mech*., ASCE, Vol.123, No.7, (b), pp.714-726.

Li, Q., & Ansari, F., 1999, "Mechanics of damage and constitutive relationships for high-strength concrete in triaxial compression," *J. Eng. Mech.*, ASCE, V.125, No.1, pp.1–10.

Menetrey, Ph., & Willam, K. J., 1995, "Triaxial failure criterion for concrete and its generalization," *ACI Struc. J*., V.92, pp.311–318.

Papanikolaou, V. K., & Kappos, A. J., 2007 "Confinement-sensitive plasticity constitutive model for concrete in triaxial compression," *Int. J. of Solids and Str*., V.44, pp.7021-7048.

Pramono, E. & Willam, K. J., 1989 "Fracture energy-based plasticity formulation of plain concrete," *J. of Engrg. Mech*., ASCE. V.115, No.6, pp.1183-1204.Smith, S. S. & Willam, K. J. & Gerstle, K. H. & Sture, S., "Concrete over the top, or is there life after the peak?," *ACI Mater. J*., V.86, 1989, pp.491–497.

Sfer . D., Carol, I., Gettu, R., & Etse, G., 2002, "Study of the Behavior of Concrete under Triaxial Compression," *J. of Engrg. Mech*., ASCE, V.128, No. 2, pp.156-163.

Stankowski, T., & Gerstle, K. H., 1985 "Simple formulation of concrete behavior under multiaxial load histories," *ACI Struc. J.*, V.82, pp.213-221.

Van Mier, J. G. M., "Multiaxial Strain-Softening of Concrete, Part I: Fracture, Part II: Load-Histories," *Materials and Structures*, RILEM, V. 19, No. 111,1986, pp. 179-200.

Vonk, R. A., 1992 "Softening of Concrete Loaded in Compression," Ph.D. thesis, Eindhoven University of Technology, the Netherlands.

Willam, K. J., & Warnke, P., "Constituve model for triaxial behavior of concrete." Seminar, Concrete Structures Subjected to Triaxial Stresses, ISMES, Bergamo, Italy, IABSE-Report No.19, III, pp.1-30.